

Long-term evolutions of the cyclotron line energies in Her X-1, Vela X-1 and Cen X-3 as observed with *Swift*/BAT

L. Ji^{1*}, R. Staubert^{1†}, L. Ducci^{1‡}, A. Santangelo^{1§}, S. Zhang^{2¶}, Z. Chang²

¹ *Institut für Astronomie und Astrophysik, Kepler Center for Astro and Particle Physics, Sand 1, D-72076 Tübingen, Germany*

² *Key Laboratory for Particle Astrophysics, Institute of High Energy Physics, Beijing 100049, China*

Accepted XXX. Received YYY; in original form ZZZ

ABSTRACT

We study the long-term evolution of the centroid energy of cyclotron lines - often referred to as Cyclotron Resonance Scattering Features (CRSF) - in Her X-1, Vela X-1 and Cen X-3, using survey observations of the Burst Alert Telescope (BAT) onboard *Swift*. We find a significant decrease of the fundamental CRSF energy in Her X-1 and the first harmonic line energy in Vela X-1, since the launch of *Swift* in 2004 and until 2010 and 2012, respectively. In both sources the decreases stopped at some time, with a quite stable centroid energy thereafter. Unlike in Her X-1 and Vela X-1, the CRSF energy in Cen X-3 does not show a long-term decrease. It is observed not to change for at least the past 14 years. The long-term variation of the line energy is a direct way to investigate the magnetic field structure in the polar regions of pulsars. Our results may stimulate the development of theoretical models, especially regarding to how the accreted mass accumulates in the accretion mound or how the magnetic field distorts around the polar cap.

Key words: X-rays: binaries; stars: neutron; stars: magnetic field; radiation mechanisms: thermal; scattering; X-rays: individual: Her X-1, Vela X-1, Cen X-3

1 INTRODUCTION

Accretion powered X-ray pulsars are some of the brightest sources in our Galaxy. Their magnetic fields are believed to be of the order of $\sim 10^{11}$ - 10^{13} G. The accreting matter is funnelled from the magnetospheric radius to a small region on the surface of the neutron star (the polar cap, see, e.g., Basko & Sunyaev 1976). In the presence of a strong magnetic field, the energies of the electrons with respect to their movement perpendicular to the magnetic field are quantized into discrete Landau levels. Resonant scattering of photons on such electrons in the line-forming region, results in cyclotron resonance scattering features (CRSFs) simply referred to as cyclotron lines. The centroid cyclotron line energy is $E_{\text{cyc}} = 11.6nB_{12}(1+z)^{-1}$, where the B_{12} is the magnetic field strength in units of 10^{12} Gauss and z is the gravitational redshift in the line-forming region. $n=1$ and $n=2,3,4,\dots$ correspond to the fundamental and harmonic cy-

clotron lines, respectively¹. Cyclotron lines provide a direct measure of the magnetic field strength in the line-forming region, and its variability reflects the changes of the accretion geometry and/or the re-arrangement of the magnetic field configuration (see, e.g., Becker et al. 2012; Mushtukov et al. 2015).

It has been found that the CRSF energy generally depends on pulse phase, often on luminosity (see, e.g., Staubert et al. 2007; Klochkov et al. 2011; Vasco et al. 2013; Fürst et al. 2014; Vybornov et al. 2017). In addition, the long-term time dependence was discovered by Staubert et al. (2014, 2016) in Her X-1, in which the cyclotron line energy decreases by ~ 5 keV over 20 years. They used the data obtained with several X-ray observatories (*RXTE*, *Beppo-SAX*, *INTEGRAL*, *Suzaku* and *NuSTAR*), in the time period from 1996 to 2015. Subsequently, Klochkov et al. (2015) independently confirmed this result by using monitoring *Swift*/BAT observations. What is more interesting is that recently Staubert et al. (2017) proposed that the 20-year E_{cyc} decrease has ended and an inverse trend could start soon. In this paper, we have started a detailed re-analysis of *Swift*/BAT data extending to the most

* E-mail: ji.long@astro.uni-tuebingen.de

† E-mail: staubert@astro.uni-tuebingen.de

‡ E-mail: ducci@astro.uni-tuebingen.de

§ E-mail: andrea.santangelo@uni-tuebingen.de

¶ E-mail: szhang@ihep.ac.cn

¹ In this paper, we quote the fundamental and the first harmonic as E_{cyc} and $E_{\text{cyc,H}}$, respectively.

recent observations, in order to follow the evolution of the cyclotron line energies over time. In addition to Her X-1, a second source was found - Vela X-1 - showing a similar long-term decrease of its first harmonic cyclotron line energy (La Parola et al. 2016). *Swift*/BAT data of Vela X-1 were analysed with the software BAT_IMAGER (Segreto et al. 2010), and it was found that the first harmonic cyclotron line decreased by ~ 0.72 keV yr $^{-1}$ between December 2004 and June 2010, and then remained constant. Additionally, there are two other candidates showing CRSF variations with time: V0332+53 and 4U 1538-22. The former shows, in its 2015 outburst, a systematically lower cyclotron line energy in the declining phase of the outburst compared to the rising phase for equal levels of luminosity (Cusumano et al. 2016; Doroshenko et al. 2017; Vybornov et al. 2017). For 4U 1538-22 a possible increase by ~ 1.5 keV may have happened between the *RXTE* and *Suzaku* observations, which are about ~ 8.5 years apart (Hemphill et al. 2016).

In this work, we re-analyze *Swift*/BAT monitoring observations of Her X-1 and Vela X-1 by using a procedure and software developed by Klochkov et al. (2015), which had led to the confirmation of the long-term decrease of the cyclotron line energy in Her X-1. We improve previous studies in four aspects:

- 1) Data after 2015, especially in Her X-1 when the decrease trend ended, are included.
- 2) The flux-correction (see below) is taken into account in Her X-1.
- 3) Updated calibration files are employed, which improves the results for all sources.
- 4) In addition to Her X-1 and Vela X-1, we searched for a long-term variation of cyclotron line energies in other sources by using archived *Swift*/BAT data. We considered all the source in Table 1 published by Maitra (2017), however, only in Cen X-3 was it possible to detect the cyclotron line (see, e.g., Santangelo et al. 1998) with sufficient significance.

Therefore, in this paper we present the evolution of the cyclotron line energies in Her X-1, Vela X-1 and Cen X-3. The paper is organized as follows: the detailed data reduction and the corresponding results are shown in Section 2 and 3, respectively. We discuss the implication of our results in Section 4.

2 OBSERVATIONS AND DATA ANALYSIS

Swift/BAT is a coded aperture telescope operating in the 15–150 keV range (Barthelmy et al. 2005). The data we selected have been taken in the *survey* mode, for which events were collected in the detector plane histograms (DPHs), typically with a five-minute exposure time. All data available since the launch of the mission in 2004 have been used. In this paper, we generally followed the data reduction of Klochkov et al. (2015). Here we briefly summarize the procedures. We reconstructed the sky map in each observation with the tools *batbinevt* and *batftimage* from the HEASOFT VER. 6.21 package². We extracted the spectra only if the source could be identified in the sky map. We used the *beterebin* tool to correct the gain/offset of detectors with

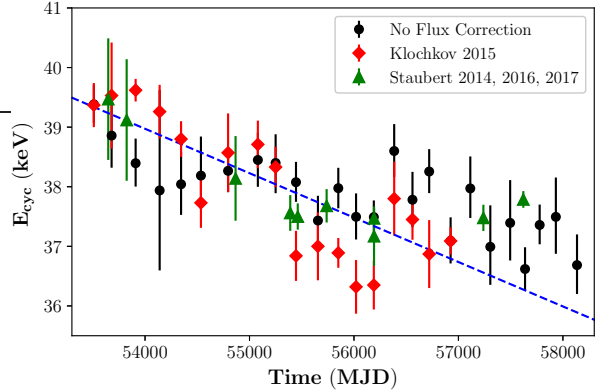


Figure 1. The long-term evolution of the CRSF energy in Her X-1 observed by *Swift*/BAT. The black and red points are the results in this paper (without the flux correction, see text) and previous results reported by Klochkov et al. (2015), respectively. The green points are taken from Staubert et al. (2014, 2016, 2017), which are observed with *RXTE*, *INTEGRAL*, *Suzaku* and *NuSTAR*. The blue dashed line is taken from Staubert et al. (2014) as well, which represents the long-term decrease of the centroid energy of the CRSF.

the latest CALDB that was released in October 2017. As suggested by the BAT team, we added the energy-dependent systematic errors by using the *batphasyserr* tool. In order to model the cyclotron line, we used a Gaussian absorption line (*gabs* in XSPEC, i.e., $\exp\left\{-\frac{\text{Depth}}{\sqrt{2\pi}\sigma}e^{-\frac{1}{2}\frac{(E-E_{\text{cyc}})^2}{\sigma^2}}\right\}$).

This model has been widely used to describe cyclotron lines (e.g., Staubert et al. 2007; Fürst et al. 2013). For the continuum, different functions were used for different sources (see below). The energy band used for the fits is 15–70 keV. To enhance the statistics in the spectral analysis, we jointly fitted tens to hundreds of spectra in a given time interval, for which the spectral shapes were assumed to be the same while normalizations were variable. The validity of this method has been verified by Klochkov et al. (2015). In this paper, all uncertainties quoted correspond to a 68% confidence level.

3 RESULTS

3.1 Her X-1

We summed the BAT spectra into time intervals based on Table 1 in Klochkov et al. (2015), and extended to new observations. We fitted the spectra with a *highcut*³ model, i.e., a power-law continuum with an exponential cut-off, modified by the CRSF component (*gabs*). This continuum model has been widely used for the long-term CRSF evolution (see, e.g., Staubert et al. 2014). Thanks to the stable continuum shape of Her X-1, we froze the parameters at the e-folding energy $E_{\text{fold}}=10$ keV, the cutoff energy $E_{\text{cut}}=21$ keV, and the powerlaw index $\Gamma = 0.9$ (Fürst et al. 2013). We show the best-fitting CRSF energy values in Figure 1, together with previous results of Klochkov et al. (2015) and Staubert et al. (2014, 2016, 2017). We found that the line energy in this paper was systematically different from that

² <https://heasarc.gsfc.nasa.gov/docs/software/lheasoft/>

³ <https://heasarc.gsfc.nasa.gov/xanadu/xspec/manual/node238.html>

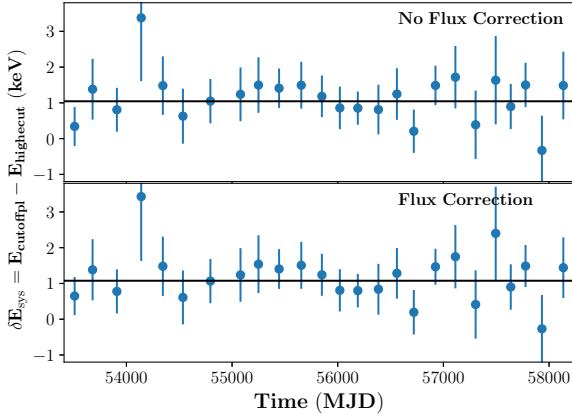


Figure 2. The systematic difference (δE_{sys}) of the detected CRSF centroid energy by using different continuum models, i.e., *highcut***powerlaw* and *cutoffpl*. On average the latter results in a higher E_{cyc} by 1.08 ± 0.10 (1.04 ± 0.10) keV if the flux correction is (not) considered.

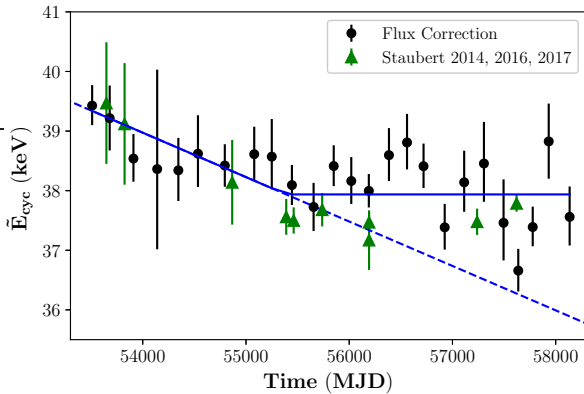


Figure 3. The long-term evolution of the CRSF energy in Her X-1 observed by *Swift*/BAT. The black points are the results of this analysis (including the flux correction, see text). The green points are taken from Staubert et al. (2014, 2016, 2017), which are observed with *RXTE*, *INTEGRAL*, *Suzaku* and *NuSTAR*. The blue dashed line is taken from Staubert et al. (2014), which represents the long-term decrease of the centroid energy of the CRSF. After the end of the decrease, the mean cyclotron line energy seems to be constant at $E_{\text{cyc}} = 37.94 \pm 0.12$ keV.

reported by Klochkov et al. (2015), although the same data and fitting method were used. We note that there are two main reasons: 1) the continuum models have a slight influence on the line detection. We fitted the spectra with two continuum models, i.e., the *highcut* and the *cutoffpl* (a power law with high energy exponential rolloff) used by Klochkov et al. (2015), and found that on average the latter resulted in a systematically higher E_{cyc} by $\delta E_{\text{sys}} = 1.04 \pm 0.10$ keV. We show the comparison in Figure 2. 2) we used the updated detector gain calibration of *Swift*/BAT in this paper, which had $\sim 4\%$ gain shift during 2004-2011. Therefore, the resulting shift of the cyclotron line energy is $\delta \text{gain} \times E_{\text{cyc}}$. We compared the expected shift with observations by using a χ^2 -test, which leads to a reduced- χ^2 of

1.2 (18 dof) with a p-value of 0.25. This suggests that the CRSF energy reported in this paper is well in agreement with that detected by Klochkov et al. (2015) after considering the above discussed two effects. In addition, it is worth noting that the CRSF energy starts to significantly deviate from the downwards trend since \sim MJD 56500, which is consistent with *NuSTAR* observations, i.e., the last two green points in Figure 1.

It is well-known that in Her X-1 the CRSF energy is related to the luminosity (L_x) (Staubert et al. 2007, 2016). Therefore, in the following spectral analysis we took the E_{cyc}/L_x correlation into account, by using the maximum flux of the individual 35d Main-On cycle from which the data were taken as a reference. Historically, the maximum Main-On flux, as measured by *RXTE*/ASM in the energy range of 2–10 keV, was taken as a measure of L_x of this particular 35d cycle (see, e.g., Staubert et al. 2007). In this paper we follow this approach, using flux measurements by *Swift*/BAT, which are converted into units of ASM-cts/s according to the following formula: (2–10 keV ASM-cts/s) = $93 \times (15\text{--}50 \text{ keV BAT-cts/s cm}^{-2} \text{ s}^{-1})$ (for details see Appendix A.2. in Staubert et al. 2016). The $E_{\text{cyc}}/\text{luminosity}$ correlation is $\delta E_{\text{cyc}} \propto f \times \delta \text{Flux}$, where f is a scaling factor allowing to normalize the measured cyclotron line energy to a reference flux. Following Staubert et al. (2014), the reference flux is $\text{Flux}_{\text{ref}} = 6.8$ ASM-cts/s, where the CRSF energy is assumed to be E_{ref} . For data until 2012 (i.e., MJD 55927) we used the scaling factor 0.44 keV/ASM-cts/s as stated by Staubert et al. (2016, 2017). For data after 2012 we used a scaling factor of 0.70 keV/ASM-cts/s, which was found to describe the data from 2012 to February 2018 with high precision (private communication with Staubert).

Generally, one point shown in Figure 1 comprises tens to hundreds of spectra from several 35d cycles. Since different 35d cycles have different maximum Main-On fluxes, the combined fitting of those spectra was done by applying appropriate scaling factors to spectra from different 35d cycles (which can easily be done within the XSPEC fitting software). So, for a spectrum (S_i), its CRSF energy could be written as $E_{\text{cyc},i} = E_{\text{ref}} + (\text{Flux}_i - \text{Flux}_{\text{ref}}) \times f$, where the Flux_i is the maximum flux of the corresponding 35d Main-On. The E_{ref} can be regarded as a fitting parameter in the spectral analysis. In this way we have obtained the long-term evolution of the cyclotron line energy for the reference flux ($\text{Flux}_{\text{ref}} = 6.8$ ASM-cts/s), i.e., the flux-corrected \tilde{E}_{cyc} . We show the result in Fig. 3. For comparison, we also include the line energies measured by other satellites as reported by Staubert et al. (2014, 2016, 2017). It is evident that the line energy decreases until a certain time t_{crit} , which is in good agreement with previous reports (the blue dashed line). After that, the line energy significantly deviates from the linear decreasing trend, and in general remains unchanged. We note that an alternative continuum model *cutoffpl* only leads to a systematically higher line energy by 1.08 ± 0.10 (Figure 2), and does not have an influence on the trend. We used a break line to fit the flux-corrected \tilde{E}_{cyc} evolution of *Swift* observations as

$$\tilde{E}_{\text{cyc}}(t) = \begin{cases} E_0 + b \times (t - t_0), & t \leq t_{\text{crit}} \\ \text{const} = E_0 + a \times (t_{\text{crit}} - t_0), & t > t_{\text{crit}} \end{cases} \quad (1)$$

where $t_0 = \text{MJD } 53500$, $E_0 = 39.88$ keV and $b = -7.22 \times 10^{-4}$ keV/d by following Staubert et al. (2014). The result-

ing t_{crit} is MJD 55400 ± 200 , and the corresponding \tilde{E}_{cyc} after t_{crit} is at 37.94 ± 0.12 keV, showing as the horizontal blue line in Figure 3. We note, that this value is systematically higher (by 0.32 keV) than the mean of *NuSTAR* and *Suzaku* observations (i.e., the green points) after t_{crit} ⁴.

3.2 Vela X-1

Following La Parola et al. (2016), we employed a Comptonization model (*compTT* in XSPEC) to describe the continuum of Vela X-1. We note that the fundamental line around 28 keV cannot be detected by BAT in Vela X-1, and in this paper we only concentrate on the first harmonic $E_{\text{cyc,H}}$. Following the above procedures, we extracted the spectra of Vela X-1, and did the spectral analysis. Although observed by La Parola et al. (2016) and Fürst et al. (2013) that the $E_{\text{cyc,H}}$ is related to the luminosity in Vela X-1, their relation has not been well constrained yet (other than in Her X-1). Therefore, in the following analysis, we did not consider the flux-correction. Actually, as shown above, the flux-correction has little influence on the trend of the cyclotron line evolution detected by BAT because the stochastic variability of the luminosity is expected to be mitigated. During the spectral analysis, we fixed the temperature of seed photons at $kT_{\text{seed}} = 1$ keV, because of no energy coverage below 15 keV for BAT. We show the results in Table A2 and Figure 4. For the sake of comparison, we divided the observations into five epochs, the first four of which were already defined in La Parola et al. (2016). The line energy decreased significantly in the first two epochs, remaining almost unchanged thereafter. Therefore, we tried to fit the line evolution with a piecewise function as mentioned above. The critical point is around MJD 55980 (February 2012). Before MJD 55980, the decrease rate of $E_{\text{cyc,H}}$ is -0.51 ± 0.09 keV per year. The $E_{\text{cyc,H}}$ after MJD 55980 is 54.96 ± 0.19 keV. In addition, it seems that there is a hump around MJD ~ 55000 . We fitted the $E_{\text{cyc,H}}$ variation with a multi-segment function (the black dashed line in Figure 4), however, the confidence level of the presence of a hump is only at 1.9σ , estimated by an F-test. Apart from the $E_{\text{cyc,H}}$, we also found a hint that the width σ_{H} might be variable. We fitted the σ_{H} evolution with a constant and a quadratic function, respectively. An F-test shows that the latter is better at a 3.5σ confidence level. We confirmed that the source of the variability of σ_{H} is not instrumental because such a trend did not appear in other sources.

3.3 Cen X-3 and other sources

We tried to apply the above method in more sources. We considered the source list in Table 1 in Maitra (2017) as a reference. We only considered persistent sources that could show the smooth long-term evolution of CRSFs. However, we found that most of sources (except for Cen X-3 and GX 301-2) could not be identified from the mosaic which was a prerequisite for extracting spectra, mainly because of the sensitivity of BAT. We found that the minimum flux to be

⁴ The comparison of the blue and the green points in Fig. 3 later that MJD 55400 may point to a calibration issue between *NuSTAR/Suzaku* and *Swift/BAT*

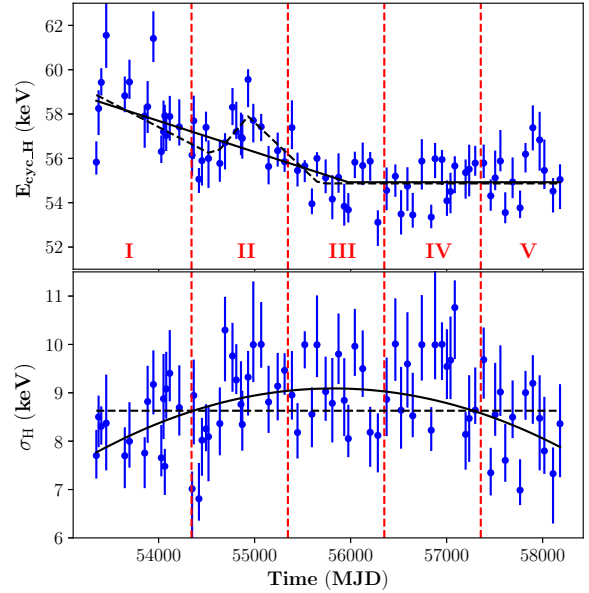


Figure 4. Upper panel: the long-term evolution of the centroid energy of the harmonic CRSF in Vela X-1 observed with *Swift*/BAT. For the sake of comparison, we divided the observations into five epochs, the first four of which were defined in La Parola et al. (2016). The line energy decreases significantly in the first two or three epochs with a rate of -0.51 ± 0.09 keV. After that, it remains almost unchanged. In addition, there seems to be a hump around the time MJD ~ 55000 , although the corresponding significance is only 1.9σ by comparing the solid and dashed black lines. Bottom panel: the long-term evolution of the CRSF width. We fitted the points with a constant line (dashed line) and a quadratic function (solid line), respectively. We found that the latter resulted in a better fitting at 3.5σ confidence level, which hinted that the width might be variable as well besides the $E_{\text{cyc,H}}$.

detected in one DPH in the survey mode is approximately $0.02 \text{ cts s}^{-1} \text{ cm}^{-2}$, i.e., 90 mCrab. In GX 301-2, we could not constrain the cyclotron line, even if different continuum models were tested. This might be due to the dramatic changes of the CRSF in GX 301-2 with different orbital phases and pulse phases (see, e.g., Kreykenbohm et al. 2004; La Barbera et al. 2005; Suchy et al. 2012), which might wipe out the absorption if stacking hundreds of spectra during fits.

In Cen X-3, the cyclotron line can be constrained well. Here we used a Fermi-Dirac (*fdcut*) function to describe the continuum following Suchy et al. (2008), where $fdcut(E) = AE^{-\Gamma} \frac{1}{1 + e^{(E - E_{\text{cut}})/E_{\text{fold}}}}$. We show the best-fitting results in Table A3 and Figure 5. Unlike the variability in Her X-1 and Vela X-1, we found that the centroid line energy in Cen X-3 was very stable over the past 14 years, at approximately 31.6 ± 0.2 keV.

4 SUMMARY AND DISCUSSION

We searched for the long-term evolution of cyclotron line parameters in persistent sources by using archived *Swift*/BAT data. Because of the regular visiting and the large field-of-view, BAT provides nearly homogeneously spaced observa-

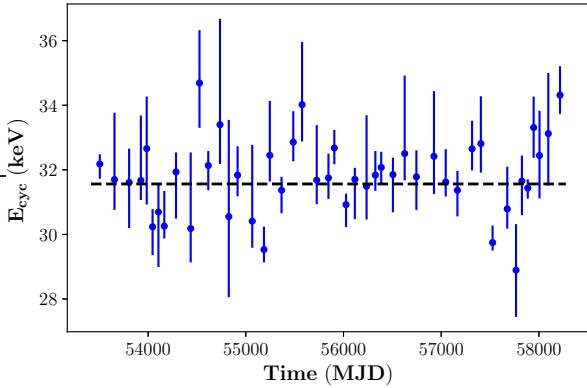


Figure 5. The long-term evolution of the CRSF in Cen X-3 observed with *Swift*/BAT.

tions without long time gaps, which is a proper instrument for monitoring CRSFs in bright sources. In Her X-1, Vela X-1 and Cen X-3, we detected cyclotron lines well, and found significant line decreases in the first two sources.

For Her X-1, we confirmed the results of Klochkov et al. (2015), while including two improvements: 1) We considered the flux-correction in the spectral analysis, which turned out to slightly influence the E_{cyc} values. 2) We analysed the data in the recent 4 years, which implied that the decrease of the CRSF centroid energy had ended around 2010 and remained constant around 37.94 ± 0.12 keV afterwards. Staubert et al. (2016, 2017) reported the continued decrease of the line energy until August 2015, when a particularly low flux was measured. With the above mentioned change of the flux correction factor (to 0.7 instead of 0.44 keV/ASM-cts/s) the flux corrected \tilde{E}_{cyc} for August 2015 is shifted upwards, leading to an estimate for the end of the decrease around 2012 to 2013 (Staubert et al., in preparation), which is consistent with the result derived here. This, in turn, indicates that the long-term \tilde{E}_{cyc} decrease observed by BAT is robust because it is not so sensitive to the flux-correction factor by averaging many spectra in different fluxes. In Vela X-1, we independently confirmed the decrease of the energy of the first cyclotron harmonic reported by La Parola et al. (2016) by using different methods. The decrease rate is 0.51 ± 0.09 keV yr $^{-1}$, which is similar to the decrease rate of ~ 0.72 keV yr $^{-1}$ stated by La Parola et al. (2016). In addition to the centroid energy, we also found a long-term variation of the width of the cyclotron line, although the validity should be further confirmed by other observatories. We also searched for the cyclotron lines in other sources, but only in Cen X-3 it is well detected. The line energy in Cen X-3 is very stable at least since 2004.

The variation of the cyclotron line energy (and width) observed in Her X-1 and Vela X-1 is believed to be caused by a local effect around the magnetic polar cap. As summarized by Staubert et al. (2014), the variation might be due to a geometric displacement of the line-forming region, or a change of the local magnetic configuration. For example, the accreting matter accumulated in the accretion mound, gradually resulting in a more extended line-forming region that corresponds to a lower magnetic field. On the other hand, the magnetic field might be changed because of

the drag by the accretion material (Cheng & Zhang 1998; Zhang & Kojima 2006), and the Hall drift and the Ohmic dissipation (Goldreich & Reisenegger 1992). However, as far as we know, no model gives a conclusive explanation of the decrease of the cyclotron line energy. More observations and theoretical works should be accumulated to investigate the complex magnetic field around the polar cap.

The time scale of the decrease of the line energy ($-E_{\text{cyc}}/E_{\text{cyc}}$) in Her X-1/Vela X-1 is ~ 100 years which is significantly shorter than the characteristic time scale of the magnetic field evolution in pulsars (Bhattacharya et al. 1992). Therefore, as suggested by Staubert et al. (2014), the centroid energy of E_{cyc} may be cyclic on time scales of a few tens to hundreds of years, which may comprise of declining, stable and rising phases. The results presented in this work show that BAT is a proper instrument to observe CRSFs in relatively bright sources such as Her X-1, Vela X-1, and Cen X-3, and supports the need for more sensitive and regular long-term monitoring of CRSFs in other accreting pulsars with observatories such as *NuSTAR*, *INTEGRAL*, *HXMT* and *Astrosat*.

ACKNOWLEDGEMENTS

JL thanks the support from the Chinese NSFC 11733009. ZS thanks the support from XTP project XDA 04060604, the Strategic Priority Research Programme 'The Emergence of Cosmological Structures' of the Chinese Academy of Sciences, Grant No.XDB09000000, the National Key Research and Development Program of China (2016YFA0400800) and the Chinese NSFC 11473027 and 11733009. We acknowledge discussions with Dr. Klochkov Dmitry, Dr. Markwardt Craig and Dr. Amy Lien, and help from the *Swift* Helpdesk.

REFERENCES

- Barthelmy S. D., et al., 2005, *Space Sci. Rev.*, **120**, 143
 Basko M. M., Sunyaev R. A., 1976, *MNRAS*, **175**, 395
 Becker P. A., et al., 2012, *A&A*, **544**, A123
 Bhattacharya D., Wijers R. A. M. J., Hartman J. W., Verbunt F., 1992, *A&A*, **254**, 198
 Cheng K. S., Zhang C. M., 1998, *A&A*, **337**, 441
 Cusumano G., La Parola V., D'Ai A., Segreto A., Tagliaferri G., Barthelmy S. D., Gehrels N., 2016, *MNRAS*, **460**, L99
 Doroshenko V., Tsygankov S. S., Mushtukov A. A., Lutovinov A. A., Santangelo A., Suleimanov V. F., Poutanen J., 2017, *MNRAS*, **466**, 2143
 Fürst F., et al., 2013, *ApJ*, **779**, 69
 Fürst F., et al., 2014, *ApJ*, **780**, 133
 Goldreich P., Reisenegger A., 1992, *ApJ*, **395**, 250
 Hemphill P. B., et al., 2016, *MNRAS*, **458**, 2745
 Klochkov D., Staubert R., Santangelo A., Rothschild R. E., Ferrigno C., 2011, *A&A*, **532**, A126
 Klochkov D., Staubert R., Postnov K., Wilms J., Rothschild R. E., Santangelo A., 2015, *A&A*, **578**, A88
 Kreykenbohm I., Wilms J., Coburn W., Kuster M., Rothschild R. E., Heindl W. A., Kretschmar P., Staubert R., 2004, *A&A*, **427**, 975
 La Barbera A., Segreto A., Santangelo A., Kreykenbohm I., Orlandini M., 2005, *A&A*, **438**, 617
 La Parola V., Cusumano G., Segreto A., D'Ai A., 2016, *MNRAS*, **463**, 185
 Maitra C., 2017, *Journal of Astrophysics and Astronomy*, **38**, 50

- Mushtukov A. A., Suleimanov V. F., Tsygankov S. S., Poutanen J., 2015, *MNRAS*, **447**, 1847
- Santangelo A., del Sordo S., Segreto A., dal Fiume D., Orlandini M., Piraino S., 1998, *A&A*, **340**, L55
- Segreto A., Cusumano G., Ferrigno C., La Parola V., Mangano V., Mineo T., Romano P., 2010, *A&A*, **510**, A47
- Staubert R., Shakura N. I., Postnov K., Wilms J., Rothschild R. E., Coburn W., Rodina L., Klochkov D., 2007, *A&A*, **465**, L25
- Staubert R., Klochkov D., Wilms J., Postnov K., Shakura N. I., Rothschild R. E., Fürst F., Harrison F. A., 2014, *A&A*, **572**, A119
- Staubert R., Klochkov D., Vybornov V., Wilms J., Harrison F. A., 2016, *A&A*, **590**, A91
- Staubert R., Klochkov D., Fürst F., Wilms J., Rothschild R. E., Harrison F., 2017, *A&A*, **606**, L13
- Suchy S., et al., 2008, *ApJ*, **675**, 1487
- Suchy S., Fürst F., Pottschmidt K., Caballero I., Kreykenbohm I., Wilms J., Markowitz A., Rothschild R. E., 2012, *ApJ*, **745**, 124
- Vasco D., Staubert R., Klochkov D., Santangelo A., Shakura N., Postnov K., 2013, *A&A*, **550**, A111
- Vybornov V., Klochkov D., Gornostaev M., Postnov K., Sokolova-Lapa E., Staubert R., Pottschmidt K., Santangelo A., 2017, *A&A*, **601**, A126
- Zhang C. M., Kojima Y., 2006, *MNRAS*, **366**, 137

**APPENDIX A: BEST-FITTING SPECTRAL
PARAMETERS IN HER X-1, VELA X-1 AND
CEN X-3**

Table A1: Best-fitting parameters of Her X-1 observed with *Swift*/BAT. E_{cyc} , σ and Depth are the energy, width and depth of the CRSF. The continuum is a powerlaw with a high energy cutoff (*highcut*), where the parameters are frozen at $\Gamma=0.9$, $E_{\text{cut}}=20.8$ and $E_{\text{fold}}=10.2$ (Fürst et al. 2013). During the spectral analysis, we considered the influence of the variable flux on the CRSF (the right three columns, see text).

Time (MJD)	E_{cyc} (keV)	σ (keV)	Depth	E_{cyc} (keV)	σ (keV)	Depth
	No Flux Correction			Flux Correction		
53440-53580	39.38 ^{+0.33} _{-0.31}	4.04 ^{+0.25} _{-0.24}	6.44 ^{+0.44} _{-0.42}	39.43 ^{+0.34} _{-0.33}	4.08 ^{+0.26} _{-0.24}	6.15 ^{+0.44} _{-0.42}
53610-53750	38.86 ^{+0.55} _{-0.54}	4.11 ^{+0.37} _{-0.38}	4.74 ^{+0.52} _{-0.51}	39.22 ^{+0.55} _{-0.54}	4.11 ^{+0.37} _{-0.38}	4.74 ^{+0.52} _{-0.51}
53790-54030	38.39 ^{+0.41} _{-0.39}	4.06 ^{+0.29} _{-0.25}	5.71 ^{+0.47} _{-0.43}	38.54 ^{+0.41} _{-0.39}	4.08 ^{+0.29} _{-0.25}	5.72 ^{+0.47} _{-0.43}
54070-54210	37.94 ^{+1.69} _{-1.34}	4.30 ^{+1.24} _{-0.97}	3.57 ^{+1.14} _{-0.89}	38.36 ^{+1.67} _{-1.35}	4.29 ^{+1.21} _{-0.92}	3.56 ^{+1.13} _{-0.87}
54240-54450	38.04 ^{+0.54} _{-0.51}	3.45 ^{+0.38} _{-0.38}	4.34 ^{+0.52} _{-0.49}	38.34 ^{+0.54} _{-0.51}	3.42 ^{+0.39} _{-0.38}	4.33 ^{+0.52} _{-0.49}
54480-54590	38.19 ^{+0.66} _{-0.55}	4.26 ^{+0.49} _{-0.30}	5.05 ^{+0.65} _{-0.50}	38.62 ^{+0.64} _{-0.56}	4.30 ^{+0.47} _{-0.31}	5.08 ^{+0.64} _{-0.51}
54620-54970	38.27 ^{+0.36} _{-0.36}	3.77 ^{+0.24} _{-0.25}	5.03 ^{+0.38} _{-0.37}	38.42 ^{+0.36} _{-0.36}	3.76 ^{+0.24} _{-0.25}	5.02 ^{+0.38} _{-0.37}
55010-55150	38.45 ^{+0.46} _{-0.45}	4.12 ^{+0.31} _{-0.32}	4.95 ^{+0.44} _{-0.43}	38.61 ^{+0.46} _{-0.45}	4.12 ^{+0.31} _{-0.32}	4.94 ^{+0.45} _{-0.43}
55180-55320	38.40 ^{+0.48} _{-0.51}	4.17 ^{+0.28} _{-0.37}	4.72 ^{+0.44} _{-0.47}	38.57 ^{+0.63} _{-0.55}	4.07 ^{+0.41} _{-0.26}	4.66 ^{+0.51} _{-0.40}
55360-55530	38.08 ^{+0.34} _{-0.33}	3.97 ^{+0.25} _{-0.23}	5.44 ^{+0.38} _{-0.36}	38.09 ^{+0.34} _{-0.33}	3.99 ^{+0.23} _{-0.24}	5.42 ^{+0.37} _{-0.36}
55570-55740	37.43 ^{+0.42} _{-0.39}	4.00 ^{+0.30} _{-0.25}	4.49 ^{+0.38} _{-0.35}	37.73 ^{+0.40} _{-0.40}	4.02 ^{+0.27} _{-0.29}	4.49 ^{+0.37} _{-0.36}
55780-55920	37.98 ^{+0.34} _{-0.34}	3.98 ^{+0.23} _{-0.24}	5.79 ^{+0.40} _{-0.39}	38.41 ^{+0.35} _{-0.34}	3.98 ^{+0.25} _{-0.22}	5.80 ^{+0.41} _{-0.38}
55950-56090	37.50 ^{+0.39} _{-0.38}	3.90 ^{+0.27} _{-0.28}	5.15 ^{+0.41} _{-0.39}	38.16 ^{+0.40} _{-0.38}	3.92 ^{+0.29} _{-0.27}	5.13 ^{+0.41} _{-0.39}
56120-56260	37.49 ^{+0.28} _{-0.28}	4.04 ^{+0.19} _{-0.20}	5.49 ^{+0.30} _{-0.30}	38.00 ^{+0.28} _{-0.28}	4.03 ^{+0.21} _{-0.19}	5.47 ^{+0.31} _{-0.30}
56300-56470	38.60 ^{+0.45} _{-0.43}	4.57 ^{+0.31} _{-0.28}	6.48 ^{+0.53} _{-0.49}	38.60 ^{+0.45} _{-0.43}	4.58 ^{+0.31} _{-0.28}	6.48 ^{+0.53} _{-0.49}
56510-56610	37.78 ^{+0.47} _{-0.46}	3.80 ^{+0.32} _{-0.34}	4.93 ^{+0.49} _{-0.48}	38.81 ^{+0.47} _{-0.46}	3.79 ^{+0.34} _{-0.33}	4.90 ^{+0.50} _{-0.47}
56650-56790	38.26 ^{+0.38} _{-0.36}	4.42 ^{+0.26} _{-0.23}	6.02 ^{+0.42} _{-0.39}	38.41 ^{+0.38} _{-0.37}	4.45 ^{+0.26} _{-0.23}	6.02 ^{+0.42} _{-0.39}
56820-57030	37.09 ^{+0.40} _{-0.38}	4.04 ^{+0.31} _{-0.28}	4.19 ^{+0.34} _{-0.32}	37.38 ^{+0.39} _{-0.37}	4.04 ^{+0.30} _{-0.28}	4.20 ^{+0.34} _{-0.32}
57060-57167	37.97 ^{+0.54} _{-0.50}	4.53 ^{+0.38} _{-0.32}	6.38 ^{+0.65} _{-0.57}	38.14 ^{+0.52} _{-0.51}	4.55 ^{+0.35} _{-0.35}	6.39 ^{+0.62} _{-0.60}
57200-57410	36.99 ^{+0.70} _{-0.64}	3.20 ^{+0.53} _{-0.49}	6.42 ^{+1.13} _{-1.01}	38.46 ^{+0.70} _{-0.64}	3.19 ^{+0.53} _{-0.49}	6.39 ^{+1.13} _{-1.00}
57440-57550	37.39 ^{+0.72} _{-0.63}	4.10 ^{+0.54} _{-0.49}	5.05 ^{+0.68} _{-0.61}	37.46 ^{+0.72} _{-0.63}	4.10 ^{+0.55} _{-0.49}	4.95 ^{+0.68} _{-0.59}
57585-57690	36.62 ^{+0.36} _{-0.35}	3.52 ^{+0.29} _{-0.28}	4.66 ^{+0.39} _{-0.37}	36.66 ^{+0.36} _{-0.35}	3.50 ^{+0.29} _{-0.28}	4.66 ^{+0.39} _{-0.37}
57725-57830	37.36 ^{+0.34} _{-0.32}	3.96 ^{+0.26} _{-0.24}	5.57 ^{+0.40} _{-0.38}	37.39 ^{+0.34} _{-0.32}	3.96 ^{+0.26} _{-0.24}	5.56 ^{+0.40} _{-0.38}
57865-58000	37.49 ^{+0.66} _{-0.62}	4.24 ^{+0.46} _{-0.39}	5.45 ^{+0.69} _{-0.61}	38.83 ^{+0.64} _{-0.63}	4.40 ^{+0.41} _{-0.43}	5.71 ^{+0.67} _{-0.65}
58030-58240	36.69 ^{+0.51} _{-0.48}	3.81 ^{+0.39} _{-0.33}	4.84 ^{+0.52} _{-0.48}	37.56 ^{+0.51} _{-0.48}	3.82 ^{+0.39} _{-0.33}	4.82 ^{+0.52} _{-0.47}

Table A2: Best-fitting parameters of Vela X-1 observed with *Swift*/BAT. $E_{\text{cyc-H}}$ (keV), σ_{H} (keV) and Depth_{H} are the energy, width and depth of the harmonic CRSF, respectively. kT_{Comp} and τ_{Comp} are the temperature and the optical depth of the Comptonized continuum spectra, respectively.

Time (MJD)	$E_{\text{cyc-H}}$ (keV)	σ_{H} (keV)	Depth_{H}	kT_{Comp} (keV)	τ_{Comp}
53351-53375	55.83 ^{+0.93} _{-0.56}	7.70 ^{+0.53} _{-0.48}	17.61 ^{+2.86} _{-1.75}	6.41 ^{+0.10} _{-0.10}	16.78 ^{+1.14} _{-1.04}
53375-53403	58.25 ^{+0.82} _{-1.20}	8.50 ^{+0.44} _{-0.63}	22.05 ^{+1.94} _{-3.01}	7.68 ^{+0.18} _{-0.19}	10.64 ^{+0.56} _{-0.53}
53403-53454	59.43 ^{+0.64} _{-0.59}	8.31 ^{+0.41} _{-0.38}	18.67 ^{+1.60} _{-1.42}	6.78 ^{+0.04} _{-0.04}	15.57 ^{+0.16} _{-0.17}
53454-53588	61.55 ^{+1.46} _{-1.47}	8.37 ^{+1.00} _{-0.98}	20.43 ^{+1.00} _{-4.42}	7.53 ^{+0.16} _{-0.15}	10.94 ^{+0.48} _{-0.61}
53648-53696	58.83 ^{+0.87} _{-0.74}	7.70 ^{+0.59} _{-0.67}	16.27 ^{+2.08} _{-1.97}	7.26 ^{+0.15} _{-0.12}	11.65 ^{+0.55} _{-0.61}
53696-53855	59.44 ^{+1.01} _{-0.76}	8.00 ^{+0.81} _{-0.54}	18.08 ^{+2.34} _{-0.75}	7.17 ^{+0.15} _{-0.06}	12.43 ^{+0.29} _{-0.75}
53855-53886	57.91 ^{+0.49} _{-1.43}	7.75 ^{+0.33} _{-0.72}	15.98 ^{+1.63} _{-2.87}	6.85 ^{+0.06} _{-0.09}	14.52 ^{+0.66} _{-0.45}
53886-53945	58.33 ^{+1.15} _{-1.19}	8.82 ^{+0.74} _{-0.85}	22.68 ^{+4.37} _{-4.51}	7.80 ^{+0.20} _{-0.28}	10.17 ^{+0.62} _{-0.45}
53945-53990	61.41 ^{+1.22} _{-1.07}	9.17 ^{+0.70} _{-0.62}	24.97 ^{+3.70} _{-3.00}	7.09 ^{+0.07} _{-0.06}	12.83 ^{+0.18} _{-0.20}
54028-54051	56.30 ^{+0.52} _{-0.52}	7.66 ^{+0.68} _{-0.38}	16.09 ^{+2.49} _{-1.11}	6.94 ^{+0.14} _{-0.11}	13.70 ^{+0.63} _{-0.62}
54051-54064	57.20 ^{+1.41} _{-0.84}	8.88 ^{+0.93} _{-0.83}	19.99 ^{+3.82} _{-3.94}	7.33 ^{+0.17} _{-0.21}	12.51 ^{+0.88} _{-0.80}
54064-54079	57.93 ^{+0.49} _{-0.90}	7.48 ^{+0.36} _{-0.59}	19.10 ^{+1.93} _{-2.51}	6.93 ^{+0.13} _{-0.11}	13.32 ^{+0.61} _{-0.77}
54079-54116	57.04 ^{+0.85} _{-0.71}	9.08 ^{+0.77} _{-0.61}	21.58 ^{+3.87} _{-2.67}	7.49 ^{+0.19} _{-0.13}	11.63 ^{+0.29} _{-0.39}
54116-54215	57.89 ^{+0.93} _{-1.09}	9.40 ^{+0.89} _{-0.58}	22.63 ^{+4.05} _{-3.53}	7.24 ^{+0.16} _{-0.19}	12.85 ^{+0.81} _{-0.53}
54215-54338	57.42 ^{+1.24} _{-0.84}	8.69 ^{+0.87} _{-0.58}	21.03 ^{+3.60} _{-2.57}	6.78 ^{+0.13} _{-0.10}	15.17 ^{+1.15} _{-0.79}
54349-54366	56.15 ^{+0.58} _{-0.94}	7.01 ^{+0.36} _{-1.09}	14.47 ^{+1.13} _{-2.85}	6.94 ^{+0.10} _{-0.14}	13.24 ^{+0.73} _{-0.68}
54366-54420	57.69 ^{+1.14} _{-1.71}	8.94 ^{+0.74} _{-1.01}	21.54 ^{+2.93} _{-5.73}	7.23 ^{+0.22} _{-0.21}	12.41 ^{+0.78} _{-0.69}
54420-54451	55.06 ^{+0.50} _{-0.62}	6.81 ^{+0.74} _{-0.45}	15.02 ^{+1.85} _{-1.81}	6.91 ^{+0.13} _{-0.10}	13.75 ^{+0.76} _{-0.94}
54451-54493	55.90 ^{+1.14} _{-1.12}	8.02 ^{+0.46} _{-0.74}	15.83 ^{+2.36} _{-2.89}	6.59 ^{+0.10} _{-0.13}	15.90 ^{+1.13} _{-1.03}
54494-54519	57.40 ^{+0.71} _{-0.64}	8.25 ^{+0.51} _{-0.46}	18.19 ^{+1.92} _{-1.64}	6.78 ^{+0.06} _{-0.05}	14.80 ^{+0.20} _{-0.22}
54519-54637	56.00 ^{+0.82} _{-1.33}	8.09 ^{+0.63} _{-0.92}	17.75 ^{+3.08} _{-2.95}	6.93 ^{+0.15} _{-0.14}	13.94 ^{+0.85} _{-0.91}
54637-54691	55.77 ^{+1.07} _{-0.83}	8.36 ^{+0.75} _{-0.66}	17.67 ^{+2.90} _{-2.62}	6.91 ^{+0.13} _{-0.12}	14.07 ^{+0.65} _{-0.94}
54691-54769	56.71 ^{+0.43} _{-1.21}	10.30 ^{+0.69} _{-1.06}	30.25 ^{+0.86} _{-6.79}	8.05 ^{+0.32} _{-0.40}	10.27 ^{+0.67} _{-0.48}
54769-54809	58.31 ^{+0.86} _{-0.81}	9.76 ^{+0.68} _{-0.74}	25.70 ^{+4.20} _{-4.49}	7.29 ^{+0.25} _{-0.25}	12.19 ^{+0.93} _{-0.88}
54809-54858	57.20 ^{+1.35} _{-0.33}	9.27 ^{+0.74} _{-0.29}	19.55 ^{+3.39} _{-1.60}	6.64 ^{+0.13} _{-0.10}	16.15 ^{+0.99} _{-0.90}
54858-54871	56.97 ^{+1.09} _{-0.82}	8.76 ^{+0.89} _{-0.48}	19.64 ^{+3.34} _{-4.34}	6.67 ^{+0.11} _{-0.12}	16.83 ^{+1.30} _{-1.14}
54871-54932	56.91 ^{+1.07} _{-0.92}	8.35 ^{+0.69} _{-0.54}	19.34 ^{+3.68} _{-2.02}	6.89 ^{+0.15} _{-0.11}	14.16 ^{+0.66} _{-0.94}
54932-54986	59.56 ^{+0.46} _{-1.25}	9.32 ^{+0.54} _{-0.79}	21.93 ^{+2.89} _{-3.10}	6.69 ^{+0.10} _{-0.09}	15.23 ^{+0.58} _{-0.88}
54986-55068	57.71 ^{+0.75} _{-0.99}	9.99 ^{+1.31} _{-0.77}	26.63 ^{+2.71} _{-4.05}	7.40 ^{+0.38} _{-0.16}	11.84 ^{+0.37} _{-0.58}
55068-55145	57.43 ^{+0.58} _{-0.65}	10.00 ^{+0.88} _{-0.48}	25.29 ^{+1.58} _{-2.42}	7.01 ^{+0.17} _{-0.08}	13.92 ^{+0.25} _{-0.34}
55145-55202	55.64 ^{+0.92} _{-0.81}	8.81 ^{+0.75} _{-0.64}	17.58 ^{+3.06} _{-2.31}	7.01 ^{+0.12} _{-0.09}	13.22 ^{+0.28} _{-0.33}
55240-55311	56.35 ^{+0.82} _{-0.72}	9.14 ^{+0.69} _{-0.71}	22.45 ^{+2.96} _{-3.56}	7.11 ^{+0.16} _{-0.20}	12.94 ^{+0.79} _{-0.82}
55312-55388	55.85 ^{+0.62} _{-0.45}	9.46 ^{+0.35} _{-0.51}	25.22 ^{+2.30} _{-2.93}	7.09 ^{+0.09} _{-0.19}	13.81 ^{+1.20} _{-0.60}
55388-55446	57.39 ^{+1.23} _{-0.97}	8.95 ^{+0.91} _{-0.51}	22.29 ^{+5.00} _{-2.80}	7.28 ^{+0.24} _{-0.15}	12.28 ^{+0.59} _{-0.84}
55447-55522	55.45 ^{+0.81} _{-0.72}	8.18 ^{+0.61} _{-0.54}	18.28 ^{+2.46} _{-2.02}	6.89 ^{+0.09} _{-0.07}	13.95 ^{+0.25} _{-0.28}
55522-55596	55.66 ^{+0.26} _{-0.73}	10.00 ^{+0.28} _{-0.49}	27.39 ^{+1.93} _{-3.10}	7.58 ^{+0.13} _{-0.24}	11.77 ^{+0.73} _{-0.34}
55597-55649	53.95 ^{+0.69} _{-0.47}	8.56 ^{+0.56} _{-0.68}	18.96 ^{+2.64} _{-3.67}	7.06 ^{+0.11} _{-0.21}	12.65 ^{+0.74} _{-0.44}
55650-55739	56.00 ^{+0.28} _{-0.82}	9.99 ^{+1.02} _{-0.67}	27.89 ^{+0.96} _{-3.91}	7.31 ^{+0.34} _{-0.17}	12.17 ^{+0.39} _{-0.46}
55740-55809	55.13 ^{+0.82} _{-0.70}	9.02 ^{+0.72} _{-0.60}	21.51 ^{+3.71} _{-2.70}	7.15 ^{+0.17} _{-0.12}	12.86 ^{+0.33} _{-0.41}
55809-55874	54.16 ^{+1.08} _{-0.91}	8.78 ^{+0.94} _{-0.81}	18.41 ^{+4.87} _{-3.53}	6.98 ^{+0.27} _{-0.21}	13.49 ^{+1.18} _{-1.03}
55874-55933	55.14 ^{+1.08} _{-1.07}	9.80 ^{+0.84} _{-0.87}	24.14 ^{+5.04} _{-2.78}	7.49 ^{+0.30} _{-0.14}	11.61 ^{+1.36} _{-0.72}
55933-55976	53.84 ^{+1.02} _{-0.87}	8.84 ^{+0.67} _{-0.74}	19.40 ^{+4.84} _{-3.56}	6.71 ^{+0.24} _{-0.19}	15.46 ^{+1.68} _{-1.38}
55976-56044	53.68 ^{+0.75} _{-0.58}	8.05 ^{+0.70} _{-0.39}	15.59 ^{+2.27} _{-2.20}	6.65 ^{+0.13} _{-0.13}	15.91 ^{+1.30} _{-0.79}
56044-56126	55.83 ^{+0.47} _{-0.71}	9.96 ^{+0.77} _{-0.61}	26.86 ^{+1.41} _{-3.41}	7.10 ^{+0.19} _{-0.14}	13.60 ^{+0.39} _{-0.35}
56126-56203	55.68 ^{+1.04} _{-0.88}	9.50 ^{+0.79} _{-0.59}	23.05 ^{+4.31} _{-3.75}	6.89 ^{+0.19} _{-0.15}	14.06 ^{+0.81} _{-0.98}
56204-56283	55.87 ^{+0.42} _{-0.88}	8.18 ^{+0.53} _{-0.71}	16.98 ^{+1.76} _{-2.25}	6.44 ^{+0.08} _{-0.14}	17.21 ^{+1.46} _{-0.94}
56283-56375	53.12 ^{+0.54} _{-1.07}	8.12 ^{+0.46} _{-0.76}	16.30 ^{+2.76} _{-3.50}	6.79 ^{+0.15} _{-0.21}	14.78 ^{+1.54} _{-0.93}
56375-56466	54.55 ^{+1.04} _{-0.89}	8.86 ^{+0.86} _{-0.76}	19.67 ^{+4.72} _{-3.55}	7.39 ^{+0.28} _{-0.23}	11.77 ^{+0.81} _{-0.73}
56466-56525	55.19 ^{+0.53} _{-0.93}	10.01 ^{+0.94} _{-0.76}	25.07 ^{+1.68} _{-4.44}	6.93 ^{+0.04} _{-0.21}	14.44 ^{+1.27} _{-0.66}
56525-56591	53.49 ^{+1.07} _{-0.92}	8.64 ^{+0.90} _{-0.80}	17.82 ^{+4.58} _{-3.41}	6.95 ^{+0.25} _{-0.20}	13.57 ^{+1.15} _{-0.99}
56592-56647	54.75 ^{+0.86} _{-1.11}	9.60 ^{+1.07} _{-0.90}	22.80 ^{+3.87} _{-4.79}	7.27 ^{+0.20} _{-0.26}	12.31 ^{+0.99} _{-0.73}
56647-56742	53.45 ^{+0.99} _{-0.58}	8.52 ^{+0.89} _{-0.44}	16.98 ^{+2.38} _{-2.87}	6.72 ^{+0.16} _{-0.17}	15.06 ^{+1.11} _{-1.06}
56742-56839	55.88 ^{+0.99} _{-1.28}	10.00 ^{+1.03} _{-0.74}	23.96 ^{+4.93} _{-5.29}	6.96 ^{+0.22} _{-0.23}	14.18 ^{+1.12} _{-0.82}
56839-56879	53.35 ^{+0.56} _{-0.50}	8.23 ^{+0.48} _{-0.43}	18.22 ^{+2.05} _{-1.69}	6.81 ^{+0.09} _{-0.08}	14.23 ^{+0.27} _{-0.29}
56880-56951	55.98 ^{+0.71} _{-0.87}	9.99 ^{+1.63} _{-0.71}	23.34 ^{+1.03} _{-3.34}	7.06 ^{+0.35} _{-0.13}	13.32 ^{+0.36} _{-0.46}
56951-57003	55.95 ^{+0.43} _{-1.15}	10.00 ^{+0.45} _{-0.74}	21.34 ^{+3.24} _{-3.52}	6.78 ^{+0.19} _{-0.15}	15.74 ^{+1.27} _{-1.15}

57003-57040	54.09 ^{+0.92} _{-0.68}	9.54 ^{+0.77} _{-0.67}	20.51 ^{+2.72} _{-3.68}	7.27 ^{+0.17} _{-0.21}	12.31 ^{+0.80} _{-0.65}
57040-57085	54.51 ^{+0.85} _{-0.98}	9.67 ^{+0.91} _{-0.80}	26.24 ^{+2.62} _{-4.91}	7.24 ^{+0.14} _{-0.26}	12.51 ^{+1.01} _{-0.75}
57085-57197	55.66 ^{+0.44} _{-1.23}	10.76 ^{+0.56} _{-1.07}	31.56 ^{+1.02} _{-7.02}	7.59 ^{+0.21} _{-0.32}	12.09 ^{+0.70} _{-0.46}
57197-57235	55.36 ^{+0.59} _{-1.18}	8.14 ^{+0.46} _{-0.73}	19.24 ^{+2.83} _{-3.39}	7.30 ^{+0.23} _{-0.20}	12.29 ^{+0.70} _{-0.89}
57235-57298	55.51 ^{+1.10} _{-1.22}	8.47 ^{+0.89} _{-0.90}	19.48 ^{+3.84} _{-3.44}	7.14 ^{+0.19} _{-0.21}	13.11 ^{+1.08} _{-0.80}
57298-57386	55.79 ^{+0.78} _{-0.57}	8.64 ^{+0.88} _{-0.28}	23.03 ^{+4.83} _{-2.30}	7.52 ^{+0.20} _{-0.10}	11.50 ^{+0.46} _{-0.65}
57386-57458	55.79 ^{+0.83} _{-0.68}	9.68 ^{+0.67} _{-0.81}	24.54 ^{+3.68} _{-3.42}	7.18 ^{+0.14} _{-0.25}	13.30 ^{+1.07} _{-0.62}
57459-57506	54.31 ^{+0.74} _{-0.67}	7.35 ^{+0.52} _{-0.47}	16.14 ^{+1.90} _{-1.64}	6.61 ^{+0.06} _{-0.05}	16.63 ^{+0.27} _{-0.28}
57506-57560	55.12 ^{+1.23} _{-0.56}	8.55 ^{+1.07} _{-0.44}	23.06 ^{+4.65} _{-2.45}	7.05 ^{+0.17} _{-0.20}	13.59 ^{+0.85} _{-0.83}
57560-57610	55.88 ^{+1.40} _{-0.47}	9.02 ^{+0.97} _{-0.49}	21.97 ^{+5.02} _{-3.05}	7.11 ^{+0.21} _{-0.22}	12.59 ^{+0.92} _{-0.78}
57610-57687	53.56 ^{+0.91} _{-0.48}	7.60 ^{+0.76} _{-0.44}	15.55 ^{+3.25} _{-2.33}	6.72 ^{+0.17} _{-0.14}	15.43 ^{+1.12} _{-1.20}
57687-57765	54.94 ^{+1.10} _{-0.73}	8.50 ^{+0.76} _{-0.43}	19.22 ^{+4.44} _{-3.69}	6.97 ^{+0.18} _{-0.20}	13.76 ^{+0.94} _{-0.86}
57765-57800	53.77 ^{+0.78} _{-0.46}	6.99 ^{+0.64} _{-0.31}	14.30 ^{+2.14} _{-1.36}	6.74 ^{+0.15} _{-0.07}	14.85 ^{+0.61} _{-1.11}
57821-57898	56.19 ^{+0.50} _{-0.83}	9.00 ^{+0.45} _{-0.56}	22.75 ^{+2.85} _{-4.43}	7.09 ^{+0.19} _{-0.19}	13.42 ^{+1.03} _{-0.82}
57898-57969	57.38 ^{+1.01} _{-1.02}	9.20 ^{+0.58} _{-0.84}	23.64 ^{+5.23} _{-4.43}	6.97 ^{+0.20} _{-0.16}	13.79 ^{+0.84} _{-0.96}
57969-58017	56.84 ^{+1.26} _{-1.39}	8.47 ^{+0.89} _{-1.08}	17.44 ^{+2.77} _{-3.47}	6.45 ^{+0.09} _{-0.11}	19.17 ^{+1.90} _{-1.32}
58018-58108	55.46 ^{+1.39} _{-0.84}	7.80 ^{+1.12} _{-0.47}	17.33 ^{+3.87} _{-2.48}	6.75 ^{+0.17} _{-0.12}	14.74 ^{+0.96} _{-1.13}
58108-58181	54.52 ^{+0.59} _{-0.96}	7.33 ^{+0.54} _{-1.03}	16.23 ^{+2.59} _{-3.31}	6.84 ^{+0.12} _{-0.14}	14.25 ^{+0.73} _{-0.89}
58181-58260	55.05 ^{+0.69} _{-1.33}	8.36 ^{+0.82} _{-1.11}	17.86 ^{+3.24} _{-4.21}	6.83 ^{+0.17} _{-0.18}	14.35 ^{+0.93} _{-1.01}

Table A3: Best-fitting parameters of Cen X-3 observed with *Swift*/BAT. E_{cyc} , σ and Depth are the energy, width and depth of the CRSF. The continuum model is a powerlaw modified by a Fermi-Dirac cutoff, where Γ and E_{fold} are the powerlaw index and the e-folding parameter.

Time (MJD)	E_{cyc} (keV)	σ (keV)	Depth	Γ	E_{fold}
53422-53595	32.18 ^{+0.30} _{-0.46}	7.17 ^{+0.70} _{-0.84}	12.44 ^{+2.37} _{-2.17}	1.35 ^{+0.07} _{-0.04}	8.55 ^{+0.39} _{-0.26}
53596-53707	31.70 ^{+2.07} _{-0.94}	7.73 ^{+2.42} _{-1.39}	11.88 ^{+9.29} _{-4.95}	1.00 ^{+0.19} _{-0.13}	6.85 ^{+0.62} _{-0.33}
53717-53889	31.61 ^{+1.05} _{-1.41}	5.35 ^{+1.17} _{-1.17}	5.87 ^{+2.06} _{-2.11}	1.84 ^{+0.16} _{-0.13}	8.72 ^{+0.53} _{-0.13}
53897-53955	31.67 ^{+2.01} _{-0.61}	4.36 ^{+1.68} _{-0.63}	4.80 ^{+2.44} _{-0.95}	1.76 ^{+0.15} _{-0.12}	8.10 ^{+0.78} _{-0.31}
53956-54015	32.66 ^{+1.61} _{-1.73}	8.69 ^{+0.97} _{-1.52}	15.46 ^{+3.64} _{-8.04}	1.11 ^{+0.18} _{-0.14}	7.22 ^{+0.84} _{-0.23}
54022-54071	30.24 ^{+0.55} _{-0.88}	2.51 ^{+0.85} _{-1.19}	1.85 ^{+0.40} _{-0.84}	2.60 ^{+0.05} _{-0.02}	12.96 ^{+1.50} _{-0.60}
54076-54135	30.69 ^{+0.87} _{-1.70}	9.96 ^{+1.98} _{-0.93}	18.50 ^{+5.13} _{-4.72}	0.95 ^{+0.16} _{-0.11}	7.14 ^{+0.56} _{-0.35}
54136-54195	30.26 ^{+1.09} _{-0.38}	6.32 ^{+0.65} _{-0.62}	8.19 ^{+1.23} _{-1.56}	1.49 ^{+0.11} _{-0.09}	8.25 ^{+0.33} _{-0.17}
54230-54366	31.94 ^{+0.60} _{-1.44}	8.04 ^{+3.77} _{-1.54}	14.14 ^{+9.64} _{-7.06}	0.93 ^{+0.12} _{-0.03}	7.36 ^{+0.61} _{-0.17}
54403-54495	30.18 ^{+2.35} _{-1.05}	6.22 ^{+2.25} _{-0.12}	9.02 ^{+5.67} _{-0.71}	0.98 ^{+0.05} _{-0.04}	7.54 ^{+1.01} _{-0.79}
54496-54545	34.69 ^{+1.64} _{-1.39}	9.99 ^{+1.49} _{-1.31}	26.18 ^{+7.61} _{-11.52}	0.90 ^{+0.17} _{-0.10}	7.81 ^{+0.93} _{-0.23}
54558-54675	32.13 ^{+0.45} _{-0.76}	6.10 ^{+0.24} _{-0.73}	8.08 ^{+0.62} _{-2.25}	1.72 ^{+0.03} _{-0.01}	8.79 ^{+0.60} _{-0.30}
54679-54777	33.40 ^{+3.27} _{-1.22}	9.98 ^{+4.13} _{-1.83}	20.20 ^{+17.24} _{-10.62}	0.86 ^{+0.16} _{-0.08}	7.17 ^{+0.92} _{-0.20}
54800-54854	30.55 ^{+2.99} _{-2.50}	9.95 ^{+0.60} _{-0.37}	15.90 ^{+5.83} _{-7.90}	0.92 ^{+0.24} _{-0.17}	6.94 ^{+0.87} _{-0.35}
54087-54975	31.84 ^{+0.90} _{-0.66}	5.41 ^{+0.82} _{-1.02}	5.66 ^{+0.88} _{-1.35}	1.86 ^{+0.15} _{-0.13}	9.52 ^{+0.49} _{-0.30}
54986-55151	30.41 ^{+2.36} _{-0.82}	9.98 ^{+5.32} _{-3.01}	17.45 ^{+22.57} _{-11.09}	0.93 ^{+0.23} _{-0.13}	7.34 ^{+0.54} _{-0.37}
55161-55215	29.53 ^{+0.71} _{-0.40}	3.37 ^{+0.33} _{-0.53}	3.02 ^{+0.55} _{-0.45}	2.22 ^{+0.13} _{-0.11}	11.00 ^{+0.63} _{-0.40}
55216-55272	32.45 ^{+1.69} _{-0.81}	9.62 ^{+3.17} _{-1.84}	18.29 ^{+12.77} _{-8.05}	0.81 ^{+0.12} _{-0.03}	6.98 ^{+0.52} _{-0.32}
55278-55452	31.37 ^{+0.42} _{-0.72}	6.19 ^{+0.67} _{-0.96}	8.10 ^{+1.14} _{-2.17}	1.57 ^{+0.08} _{-0.04}	8.55 ^{+0.53} _{-0.41}
55465-55515	32.85 ^{+0.96} _{-0.59}	7.69 ^{+1.48} _{-1.19}	15.18 ^{+3.66} _{-3.71}	1.28 ^{+0.08} _{-0.03}	8.20 ^{+0.40} _{-0.30}
55517-55631	34.02 ^{+1.95} _{-1.14}	10.02 ^{+1.57} _{-1.81}	23.03 ^{+9.37} _{-10.27}	0.94 ^{+0.19} _{-0.10}	8.04 ^{+1.03} _{-0.29}
55638-55804	31.68 ^{+1.71} _{-0.74}	9.52 ^{+3.10} _{-1.92}	16.99 ^{+10.86} _{-8.80}	1.20 ^{+0.15} _{-0.09}	7.92 ^{+0.69} _{-0.30}
55833-55875	31.75 ^{+0.75} _{-0.65}	6.33 ^{+2.91} _{-1.52}	7.99 ^{+12.19} _{-3.36}	1.30 ^{+0.12} _{-0.10}	7.74 ^{+0.38} _{-0.13}
55876-55935	32.68 ^{+0.56} _{-0.51}	9.99 ^{+0.85} _{-1.15}	20.19 ^{+2.80} _{-6.31}	1.16 ^{+0.12} _{-0.06}	7.67 ^{+0.44} _{-0.36}
55996-56055	30.92 ^{+0.34} _{-0.69}	5.48 ^{+0.51} _{-1.17}	6.01 ^{+0.80} _{-2.12}	1.44 ^{+0.16} _{-0.13}	7.77 ^{+0.48} _{-0.16}
56056-56163	31.71 ^{+0.36} _{-1.23}	6.13 ^{+0.32} _{-1.09}	7.40 ^{+0.44} _{-2.85}	1.58 ^{+0.14} _{-0.12}	8.57 ^{+0.67} _{-0.25}
56207-56278	31.49 ^{+2.20} _{-1.03}	10.00 ^{+3.98} _{-1.39}	17.24 ^{+14.38} _{-4.24}	0.83 ^{+0.09} _{-0.02}	6.96 ^{+0.46} _{-0.20}
56307-56355	31.84 ^{+0.75} _{-0.49}	7.30 ^{+0.37} _{-0.60}	10.87 ^{+1.60} _{-2.05}	1.35 ^{+0.02} _{-0.02}	7.96 ^{+0.38} _{-0.22}
56356-56413	32.07 ^{+0.49} _{-0.54}	6.62 ^{+0.42} _{-0.81}	8.33 ^{+0.46} _{-1.40}	1.66 ^{+0.14} _{-0.13}	8.49 ^{+0.38} _{-0.24}
56416-56595	31.85 ^{+0.52} _{-1.17}	7.19 ^{+0.45} _{-1.04}	11.47 ^{+0.65} _{-3.15}	0.69 ^{+0.12} _{-0.09}	6.83 ^{+0.37} _{-0.16}
56596-56631	32.50 ^{+2.41} _{-0.83}	9.37 ^{+1.95} _{-1.65}	17.95 ^{+10.68} _{-8.29}	1.22 ^{+0.17} _{-0.13}	7.65 ^{+0.84} _{-0.28}
56702-56835	31.78 ^{+0.82} _{-1.02}	9.58 ^{+1.48} _{-1.71}	16.70 ^{+5.51} _{-6.88}	0.98 ^{+0.08} _{-0.07}	7.03 ^{+0.29} _{-0.15}
56838-57008	32.42 ^{+2.02} _{-1.17}	10.00 ^{+3.05} _{-2.07}	18.32 ^{+11.84} _{-9.06}	0.74 ^{+0.12} _{-0.07}	6.94 ^{+0.60} _{-0.28}
57020-57067	31.62 ^{+1.02} _{-0.45}	8.78 ^{+0.32} _{-1.26}	14.55 ^{+1.24} _{-3.79}	0.97 ^{+0.11} _{-0.09}	7.08 ^{+0.32} _{-0.18}
57102-57246	31.37 ^{+0.60} _{-0.81}	6.74 ^{+0.94} _{-1.47}	9.04 ^{+2.39} _{-3.56}	1.50 ^{+0.14} _{-0.11}	8.73 ^{+0.38} _{-0.24}
57276-57359	32.65 ^{+0.87} _{-0.67}	9.14 ^{+1.62} _{-1.47}	17.65 ^{+5.56} _{-7.07}	1.34 ^{+0.18} _{-0.15}	8.51 ^{+0.59} _{-0.22}
57379-57405	32.81 ^{+1.47} _{-0.90}	10.00 ^{+0.23} _{-1.20}	19.82 ^{+1.78} _{-3.95}	1.16 ^{+0.08} _{-0.04}	8.14 ^{+0.60} _{-0.41}
57436-57615	29.75 ^{+0.53} _{-0.25}	6.35 ^{+1.07} _{-0.60}	6.86 ^{+1.98} _{-0.99}	1.22 ^{+0.16} _{-0.14}	7.38 ^{+0.41} _{-0.25}
57616-57735	30.79 ^{+1.31} _{-0.61}	9.32 ^{+2.76} _{-1.67}	15.12 ^{+8.55} _{-4.98}	1.31 ^{+0.17} _{-0.13}	8.09 ^{+0.65} _{-0.31}
57736-57795	28.89 ^{+1.42} _{-1.45}	10.00 ^{+1.37} _{-1.00}	14.38 ^{+4.97} _{-4.25}	0.71 ^{+0.27} _{-0.18}	6.25 ^{+0.70} _{-0.44}
57614-57851	31.65 ^{+0.79} _{-1.05}	10.02 ^{+3.67} _{-2.82}	14.44 ^{+10.37} _{-7.35}	0.69 ^{+0.20} _{-0.11}	6.48 ^{+0.60} _{-0.25}
57856-57915	31.44 ^{+0.27} _{-0.33}	7.09 ^{+0.75} _{-1.04}	11.03 ^{+1.87} _{-3.07}	1.34 ^{+0.09} _{-0.04}	8.27 ^{+0.39} _{-0.30}
57916-57956	33.31 ^{+0.96} _{-0.94}	9.26 ^{+1.78} _{-1.09}	16.41 ^{+6.83} _{-5.46}	1.10 ^{+0.15} _{-0.10}	7.54 ^{+0.41} _{-0.23}
57984-58009	32.44 ^{+1.39} _{-1.33}	8.51 ^{+0.61} _{-0.77}	14.50 ^{+4.45} _{-4.60}	1.03 ^{+0.13} _{-0.10}	7.39 ^{+0.63} _{-0.25}
58037-58155	33.12 ^{+1.88} _{-1.61}	9.96 ^{+2.33} _{-1.41}	19.24 ^{+8.02} _{-7.89}	1.12 ^{+0.07} _{-0.03}	7.91 ^{+0.85} _{-0.44}
58159-58267	34.31 ^{+0.90} _{-0.58}	8.28 ^{+0.50} _{-1.37}	16.14 ^{+1.78} _{-4.72}	1.27 ^{+0.16} _{-0.13}	8.24 ^{+0.67} _{-0.36}

This paper has been typeset from a $\text{\TeX}/\text{\LaTeX}$ file prepared by the author.